How to cite: *Angew. Chem. Int. Ed.* **2024**, *63*, e202400343
doi.org/10.1002/anie.202400343

VIP **Lithium-Sulfur Batteries** *Very Important Paper*

Anion-Involved Solvation Structure of Lithium Polysulfides in Lithium–Sulfur Batteries

Yun-Wei Song, Liang Shen, Nan Yao, Shuai Feng, Qian Cheng, Jin Ma, Xiang Chen, Bo-Quan Li, and Qiang Zhang**

Abstract: Lithium polysulfides (LiPSs) are pivotal intermediates involved in all the cathodic reactions in lithium–sulfur (Li–S) batteries. Elucidating the solvation structure of LiPSs is the first step for rational design of electrolyte and improving Li–S battery performances. Herein, we investigate the solvation structure of LiPSs and find that Li salt anions tend to enter the first solvation sheath of LiPSs and form contact ion pairs in electrolyte. The anion-involved solvation structure of LiPSs significantly influences the intrinsic kinetics of the sulfur redox reactions. In particular, the LiPS solvation structure modified by lithium bis(fluorosulfonyl)imide endows Li–S batteries with reduced polarization and enhanced rate performances under high sulfur areal loading and lean electrolyte volume conditions. This work updates the fundamental understanding of the solvation chemistry of LiPSs and highlights electrolyte engineering for promoting the performances of Li–S batteries.

[*] Y.-W. Song, L. Shen, N. Yao, J. Ma, Dr. X. Chen, Prof. Q. Zhang
Beijing Key Laboratory of Green Chemical Reaction Engineering and Technology, Department of Chemical Engineering
Tsinghua University
100084 Beijing, China
E-mail: zhang-qiang@mails.tsinghua.edu.cn

Q. Cheng, Dr. B.-Q. Li
Advanced Research Institute of Multidisciplinary Science
Beijing Institute of Technology
100081 Beijing, China
E-mail: libq@bit.edu.cn

Q. Cheng, Dr. B.-Q. Li
School of Materials Science and Engineering
Beijing Institute of Technology
100081 Beijing, China

Dr. S. Feng
College of Chemistry and Chemical Engineering
Taishan University
271021 Shandong, China

J. Ma
Shanxi Research Institute for Clean Energy
Tsinghua University
030032 Taiyuan, China

Introduction

Lithium–sulfur (Li–S) batteries, distinguished by their ultra-high theoretical energy density of 2600 $Wh\,kg^{-1}$, have been strongly considered as next-generation electrochemical energy storage devices.[1] The typical reactions within a Li–S battery include the reduction of solid sulfur (S_8) to generate a series of lithium polysulfides (LiPSs) and the formation of solid lithium sulfide (Li_2S) as the final discharge product.[2] The LiPSs serve as key intermediates in Li–S batteries that enable feasible electrochemical conversion pathways between insulating S_8 and Li_2S solids, thereby improving the utilization of active materials.[3] Despite the above merits, the excessive solubility of LiPSs results in extremely deteriorated reaction kinetics under practical working conditions such as using high-loading sulfur cathodes and lean electrolyte volume.[4] Meanwhile, the LiPSs react violently with the Li metal anode to render severe corrosion and rapid anode failure.[5] Therefore, rationally regulating the behaviors of LiPSs is of vital importance for realizing practical Li–S batteries.

Rational design of electrolyte is considered as one of the most promising solutions to address the above challenges.[6] By rationally designing the electrolyte components and modulating the solvation structure of LiPSs, one can regulate the solubility and reactivity of LiPSs and consequently optimize the overall performances of Li–S batteries.[7] Various approaches have been proposed including designing new solvents or Li salts,[8] optimizing the solvent or Li salt concentrations,[9] introducing functional additives,[10] redox mediators,[11] and developing novel ionic liquid electrolytes,[12] localized high-concentration electrolytes,[13] and LiPS encapsulating electrolytes.[14] Concurrently, multiple theoretical investigations are focusing on interpreting the role of solvents and Li salts on the solubility,[15] existing form,[16] transport properties,[17] and reaction kinetics of LiPSs.[18] However, a comprehensive understanding of the solvation structure of LiPSs, especially regarding how LiPSs interact with the electrolyte components and form specific ion–solvent complexes, remain elusive. Further exploration is requested to uncover the underlying solvation chemistry and unlock full potential of Li–S batteries.

Our previous study has found that the LiPSs in electrolyte bond with extra Li ions and mainly exist as LiPS cations.[19] In this contribution, we further investigate the solvation structure of the cationic LiPSs and reveal that Li salt anions are involved in the solvation structure of LiPSs

and significantly influence their intrinsic reaction kinetics. Specifically, the anions dissociated from Li salts form contact ion pairs with LiPS cations in electrolyte, thus participate prominently in the first solvation sheath of LiPSs (Figure 1). The anions modify the formation energy of the LiPS intermediates, thereby significantly affect the intrinsic kinetics of the sulfur redox reactions. As a proof-of-concept, Li–S batteries with the addition of lithium bis(fluorosulfonyl)imide (LiFSI) demonstrate higher discharge capacity, reduced polarization, and enhanced rate performances compared with the commonly-used lithium bis(trifluoromethanesulfonyl)imide (LiTFSI). This work deepens our understanding on the solvation chemistry of LiPSs in Li–S batteries and highlights the promising potential of electrolyte designing for constructing high-performance Li–S batteries.

Results and Discussion

The interaction between Li salts and LiPSs is firstly investigated to probe the solvation structure of LiPSs. Three sulfonimide-based Li salts with similar structures, regarding LiFSI, LiTFSI, and lithium bis(pentafluoroethanesulfonyl)imide (LiBETI), are selected as the model Li salts. Figure 2a and S1 exhibits the ^{19}F nuclear magnetic resonance (NMR) spectra of the Li salts with or without the addition of Li_2S_6 in 1,2-dimethoxyethane

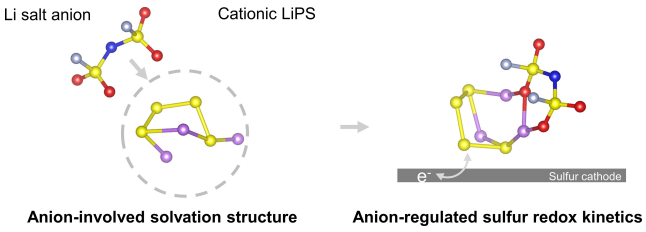

Figure 1. Schematic diagram of the anion-involved solvation structure of LiPSs. Li salt anions participate in the first solvation sheath of LiPSs and regulate the intrinsic sulfur redox kinetics. The spheres with the colors of yellow, purple, aquamarine, red, and blue correspond to S, Li, F, O, and N atoms, respectively.

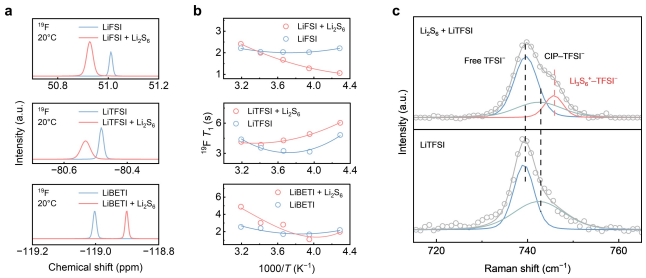

Figure 2. Spectroscopy identification of anion-involved solvation structure of LiPSs in electrolyte. a) ^{19}F NMR spectra of LiFSI, LiTFSI, and LiBETI solutions and their mixture with Li_2S_6 and b) corresponding temperature-dependent t_1 relaxation relationship. c) Raman spectra of LiTFSI solution and Li_2S_6 + LiTFSI solution.

(DME) solvent at varied temperatures. The ^{19}F NMR signal of the FSI^-, $TFSI^-$, and $BETI^-$ anions exhibits an obvious chemical shift change in the presence of Li_2S_6, indicating a unique interaction exists between LiPSs and Li salt anions that affects the electron density surrounding the F nuclei. The temperature-dependent spin–lattice (t_1) relaxation measurements were further carried out to probe the chemical environment around the F nuclei by quantifying the energy exchange rate between the F atoms and their surrounding environments (Figure 2b). Notably, both the minimum t_1 relaxation time and the corresponding temperature are significantly shifted after the addition of Li_2S_6, indicating a distinct coordination environment of the F nuclei with different local symmetry.[20] These findings manifest nonnegligible chemical interaction between Li salt anions and LiPSs and suggest the direct involvement of Li salt anions in the solvation structure of LiPSs.

To further investigate the coordination environment of LiPSs in electrolyte, Raman spectra of Li_2S_6 solution with the addition of LiTFSI were collected (Figure 2c). For the blank LiTFSI solution, the Raman signal in the wavenumber region of 730–750 cm^{-1} is assigned to the vibrational modes of $TFSI^-$ anions.[21] The Raman signal can be further deconvoluted into two components, including uncoordinated $TFSI^-$ at 739 cm^{-1} (Free $TFSI^-$), and $TFSI^-$ coordinated with Li^+ located at 742 cm^{-1} (CIP-$TFSI^-$).[22] With the addition of Li_2S_6, a new vibrational mode of $TFSI^-$ emerges at 746 cm^{-1}, indicating direct coordination of $TFSI^-$ to LiPSs. Generally, Li_2S_6 molecules in electrolyte prefer to bond with extra Li^+ and exist as cationic $Li_3S_6^+$ species.[19] Therefore, the new vibrational mode is assigned as the contact ion pair formed between $Li_3S_6^+$ and $TFSI^-$. Similar trends are also observed in LiFSI and LiBETI-based solutions with a distinct vibrational mode of $Li_3S_6^+$–FSI^- and $Li_3S_6^+$–$BETI^-$ deconvoluted at a wavenumber of 725 and 749 cm^{-1}, respectively (Figure S2 and S3).[23]

The spectroscopy studies reveal direct interaction between LiPSs and Li salt anions in electrolyte. To further confirm the anion-involved solvation structure of LiPSs and obtain detailed structural information, density functional theory (DFT) calculations were conducted to probe the interaction between LiPSs and other electrolyte components. The thermodynamic feasibility of a Li salt anion entering the first solvation sheath of LiPSs and substituting the pristine solvating DME molecule was evaluated through calculating the Gibbs free energy change (ΔG) of the ligand exchange reaction as shown in Figure 3a. The calculated ΔG values are exhibited in Figure 3b. All the formation of $Li_3S_n^+$ $-An^-$ presents a negative ΔG value from -0.3 to -0.7 eV, indicating the Li salt anions are thermodynamically favorable to substitute DME solvents and participate in the first solvation sheath of LiPSs to form contact ion pairs in electrolyte. Figure 3c, S4, and S5 exhibit the optimized structures of $Li_3S_n^+$ solvated by different Li salt anions. The two oxygen atoms of the Li salt anion are coordinated to one Li atom of $Li_3S_n^+$ in all the $Li_3S_n^+$–An^- ion pairs, forming a six-membered-ring-like structure. Meanwhile, one of the oxygen atoms is also coordinated with another Li

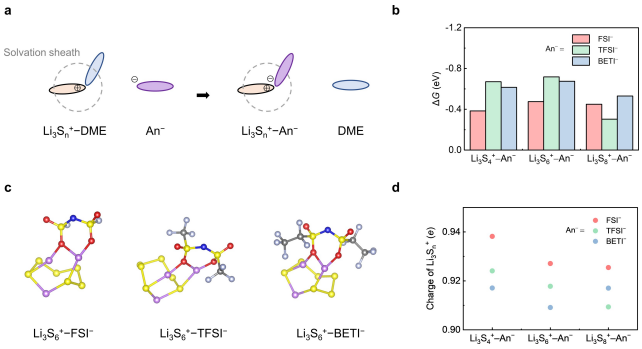

Figure 3. Theoretical calculations of anion-involved solvation structure of LiPSs in electrolyte. a) Schematic diagram of the ligand substitution reaction of $Li_3S_n^+$ by An^-. b) Calculated ΔG of the ligand substitution reaction to form $Li_3S_4^+$–An^-, $Li_3S_6^+$–An^-, or $Li_3S_8^+$–An^-. c) Optimized structure of $Li_3S_6^+$–FSI^-, $Li_3S_6^+$–$TFSI^-$, and $Li_3S_6^+$–$BETI^-$. The spheres with the colors of yellow, purple, aquamarine, red, grey, and blue correspond to S, Li, F, O, C, and N atoms, respectively. d) NBO charge of $Li_3S_n^+$ after the coordination of An^-.

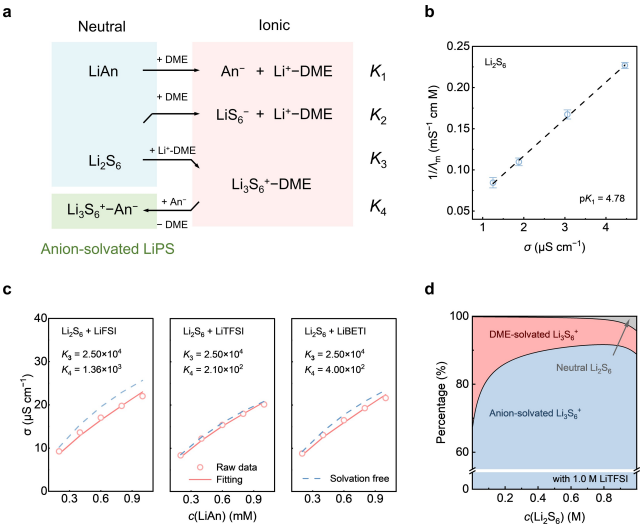

Figure 4. Quantitative analysis on the solvation structure of LiPSs. a) Dissociation and association equilibria in dilute solution of LiAn and Li_2S_6. b) Linear fitting of the conductivity of Li_2S_6 to determine the dissociation constant, K_1. c) Data fitting to determine the formation constant of anion-solvated LiPSs, K_4. d) Simulated fraction of Li_2S_6 with different solvation structures at different Li_2S_6 concentrations with the addition of 1.0 M LiTFSI.

atom, rendering strong electrostatic interaction and a compact coordination structure.

The charge transfer between $Li_3S_n^+$ and An^- was investigated through the natural bond orbital (NBO) analysis (Figure 3d). With the coordination of An^-, $Li_3S_n^+$ maintains its ionic nature with negligible net electron transfer from An^- to $Li_3S_n^+$ (<0.09 e). This suggests that the solvation effect of the anions on the LiPS cations exhibits the nature of ion–ion interaction. Compared with the ion–dipole interaction between the LiPS cations and solvents, the ion–ion interaction is typically stronger, resulting in preferential involvement of the Li salt anions into the first solvation sheath of the LiPSs.[24] Moreover, for the different Li salt anions, the order of electron transfer from An^- to $Li_3S_n^+$ reveals a progression of $FSI^- < TFSI^- < BETI^-$, suggesting enhanced electrostatic interaction with the increase of the anion radius.

The above spectroscopy studies and theoretical calculations manifest the Li salt anions prefer to directly participate in the first solvation sheath of LiPSs. Conductivity analysis was further performed to quantitatively investigate the solvation structure of LiPSs. With the addition of Li salt (denoted as LiAn), the ion dissociation and association reactions existing in dilute Li_2S_6 solution are listed in Figure 4a. These reactions include (1) the dissociation of Li_2S_6 in DME solvent to generate a LiS_6^- and a DME-solvated Li^+ (Li^+–DME), (2) the dissociation of LiAn, (3) the association between Li_2S_6 and Li^+–DME to form DME-solvated $Li_3S_6^+$ ($Li_3S_6^+$–DME), and (4) the ligand substitution reaction from $Li_3S_6^+$–DME to $Li_3S_6^+$–An^- contact ion pairs. The equilibrium constant of these reactions is denoted as K_1, K_2, K_3, and K_4, respectively. By measuring the conductivity (σ) of the dilute solutions of Li_2S_6, LiFSI, LiTFSI, and LiBETI, their dissociation constants (K_1 and each K_2 for different Li salts) can be separately determined (Figure S6 and Table S1–S4). Specifically, the value of dissociation constant can be obtained by linear fitting of the reciprocal of molar conductivity ($1/\Lambda_m$) against σ.[25] For Li_2S_6, the value of pK_1 is fitted to be 4.78, corresponding to a weak dissociation behavior in DME solvent (Figure 4b). The pK_2 values are fitted to be 4.20, 4.04, and 3.96 for LiFSI, LiTFSI, and LiBETI in DME solvent, respectively (Figure S7). The measured pK_2 values indicate that the dissociation tendency follows the order LiFSI < LiTFSI < LiBETI, which is attributed to the increased anionic radius and more dispersed negative charge on the Li salt anions.

We further measured the conductivity of the mixture solutions of Li_2S_6 and different Li salts. The compositions of the solutions are 0.50 mM Li_2S_6 with 0.20, 0.40, 0.60, 0.80, or 1.0 mM LiFSI, LiTFSI, or LiBETI, respectively. Following the ion-independent migration law in dilute solution, the conductivity of the solution can be calculated by the given equilibrium constants K_1–K_4 and limiting molar conductivity of each ion pair. Therefore, the unknown value of K_4 can be fitted for each Li salt according to the experimentally measured conductivity values. The measured conductivity and fitting results of the mixture solutions are exhibited in Figure 4c. K_4 is determined to be 1.36×10^3, 2.10×10^2, and 4.00×10^2 for the formation of $Li_3S_6^+$–FSI^-, $Li_3S_6^+$–$TFSI^-$, and $Li_3S_6^+$–$BETI^-$, respectively. Importantly, when neglecting the solvation effect of Li salt anions ($K_4=0$, blue dash line in Figure 4c), the fitting results fail to explain the conductivity variations in all the Li_2S_6 and Li salt-containing solutions, highlighting the validity of using quantitative conductivity analysis to determine K_4.

Based on the equilibrium constants, it can be concluded that Li salt anions exhibit a strong tendency to enter the first solvation sheath of LiPSs and form contact ion pairs in electrolyte. With the existence of Li salts, the fraction of LiPSs in different solvation structures, including neutral

Li_2S_6, DME-solvated $Li_3S_6^+$ cations, and anion-solvated $Li_3S_6^+$ cations, was further simulated. As shown in Figure 4d, the $TFSI^-$-solvated $Li_3S_6^+$ cations dominate in electrolyte at varied nominal concentrations of Li_2S_6 with 1.0 M LiTFSI. At low concentrations (<0.1 M), $TFSI^-$-solvated $Li_3S_6^+$ cations constitute approximately 65 %, highlighting the strong solvation effect of the Li salt anion on LiPSs. As the Li_2S_6 concentration increases to 0.6 M, the proportion of $TFSI^-$-solvated $Li_3S_6^+$ cations further rises to around 90 %. This can be attributed to an increase in the ratio of sulfur species that shifts the reaction equilibrium to the right. When the Li_2S_6 concentration further increases to 1.0 M, the elevated Li_2S_6 concentration leads to the competition of Li_2S_6 with $TFSI^-$ for Li^+ ions. Consequently, the proportion of cationic $Li_3S_6^+$ species reduces, while neutral Li_2S_6 rises to 5 %. Similar results can be observed in the systems with LiFSI or LiBETI, all performing An^--solvated $Li_3S_6^+$ cations as the main species (Figure S8). Hence, it is manifested that anion-solvated LiPS cations are the predominant existence form in electrolyte (generally over 85 %), evidencing the significant involvement of Li salt anions in the solvation structure of LiPSs in Li–S batteries.

Li salt anions significantly involve in the first solvation sheath of LiPSs and modify their molecule structure. This suggests that Li salts not only function as charge carriers in Li–S batteries but also influence the electrochemical activity of LiPSs by modulating the LiPS solvation structures. Electrochemical evaluations were conducted to evaluate the influence of the different Li salt anions on the reaction kinetics of LiPSs. Temperature-dependent electrochemical impedance spectra (EIS) were firstly measured in Li_2S_6 symmetric cells to evaluate the liquid–liquid conversion kinetics with different anions. To exclude the influence of the ratio between the cationic and neutral LiPS species and the bulk ion conductivity afforded by the different Li salts, the nominal concentrations of LiFSI, LiTFSI, and LiBETI were controlled to ensure the same equilibrium Li^+ concentration. Concretely, 100 mM Li_2S_6 with 1.5 M LiFSI, 1.0 M LiTFSI, or 0.84 M LiBETI were employed as the electrolyte according to the respective dissociation constants (K_2 measured according to the quantitative conductivity analysis). As shown in Figure 5a, S9–S10, and Table S5, Li_2S_6 with the addition of LiFSI exhibits the smallest charge transfer resistance (R_{ct}) value of 22, 8.2, 3.2, and 1.7 ohm at all the temperatures of −10 °C, 0 °C, 10 °C, and 20 °C, rendering the LiPSs undergo the fastest redox kinetics with the solvation of FSI^-. In contrast, both LiTFSI and LiBETI exhibit much higher R_{ct} values and slower reaction kinetics. Based on the Arrhenius equation, the activation energy (E_a) for Li_2S_6 conversion was further obtained (Figure 5b). The E_a values of LiFSI, LiTFSI, and LiBETI solvated Li_2S_6 are respectively determined as 55.0, 63.3, and 66.3 kJ mol^{-1}, indicating reduced energy barrier of the FSI^--solvated LiPSs in electrochemical conversions. Next, potentiostatic nucleation tests were employed to investigate the kinetics of the conversion from soluble LiPSs to solid Li_2S (Figure 5c). During the potentiostatic discharge under 2.05 V, the cell with LiFSI delivers the earliest nucleation peak at 450 s and the highest Li_2S deposition capacity of 318.3 mAh g^{-1}. In comparison,

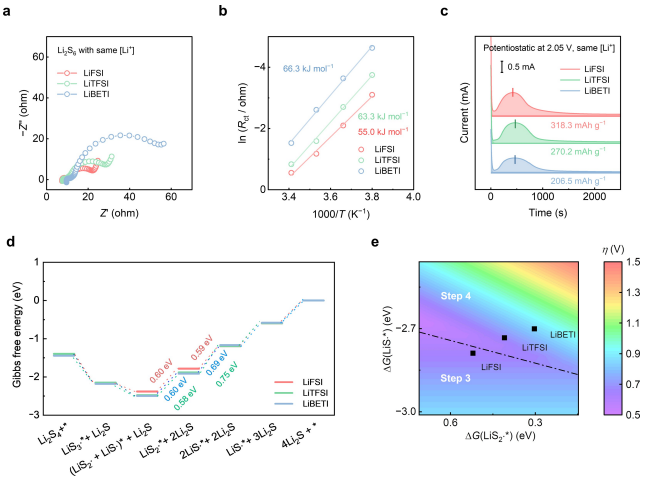

Figure 5. Kinetic evaluation on anion-solvated LiPSs. a) EIS spectra of Li_2S_6 with LiFSI, LiTFSI, or LiBETI at 0 °C. [Li^+] is controlled as the same value. b) Arrhenius plot to determine the E_a of Li_2S_6 conversion with different Li salts. c) Potentiostatic nucleation test with LiFSI, LiTFSI, or LiBETI. [Li^+] is controlled as the same value. d) Calculated Gibbs free energy diagrams of the sulfur reduction reaction from Li_2S_4 to Li_2S with different Li salts at U = 2.20 V. e) 2D volcano plot of overpotential versus ΔG(LiS·*) and ΔG(LiS_2·*).

the cells exhibit inferior nucleation kinetics with LiTFSI or LiBETI, exhibiting a delayed peak time of 520 or 527 s and lower deposition capacity of 270.2 or 266.5 mAh g^{-1}, respectively. These results indicate higher intrinsic activity of the FSI^--solvated LiPSs and reveal the kinetics order of FSI^- > $TFSI^-$ > $BETI^-$ in LiPS conversion reactions.

In order to understand the underlying chemistry of the kinetics order of the different Li salt anions, an electrocatalytic model is established through DFT calculations to probe the reaction mechanisms of the six-electron sulfur reduction reaction from Li_2S_4 to Li_2S.[26] The overall reaction is considered with six elementary steps, following an asymmetric reaction pathway that generates a series of anion-solvated LiPS radicals (Figure S11–S13). With different solvating anions, the Gibbs free energy profiles of the sulfur reduction reaction at an electrode potential of U = 2.20 V vs. Li/Li^+ are presented in Figure 5d. When $TFSI^-$ or $BETI^-$ acts as the solvating anion, step 4 exhibits the most positive ΔG and is identified the rate-determining step, with an energy barrier of 0.69 and 0.75 eV for $TFSI^-$ and $BETI^-$, respectively. In contrast, with FSI^- as the solvating anion, the ΔG value of step 4 reduces to only 0.59 eV and the rate-determining step becomes the third step (0.60 eV). These results suggest that the addition of LiFSI as Li salt reduces the activation energy barrier of the sulfur reduction reactions. Furthermore, the two-dimensional (2D) volcano plot in Figure 5e links the overpotential with the formation Gibbs free energies of LiS_2·* and LiS·* radicals, namely ΔG(LiS_2·*) and ΔG(LiS·*). From $BETI^-$ to FSI^-, a clear correlation is observed between the decreased reaction overpotential and the positive shift in ΔG(LiS_2·*) as well as the negative shift in ΔG(LiS·*). As a result, the kinetics order of FSI^- > $TFSI^-$ > $BETI^-$ is attributed to the elevated

energy of LiS_2·* and stabilized LiS·* radical that facilitates the reduction step from LiS_2·* to LiS·*. This result provides a molecular-level explanation for the mechanism that Li salt anion solvation affects the LiPS reaction kinetics intrinsically, and highlights the potential of further reaction regulation through rational Li salt anion design.

The influence of the different solvation structures on the LiPS redox kinetics indicates the feasibility of Li salt anion regulation to promote Li–S battery performances. Cyclic voltammetry (CV) was carried out to assess the kinetics in a complete charge and discharge cycle of Li–S batteries. As shown in Figure 6a, the CV curves contain two cathodic peaks (a and b) and two anodic peaks (c and d). Peaks a and b correspond to the reduction of sulfur to soluble LiPSs and the subsequent reduction to generate insoluble Li_2S. Conversely, the anodic peaks c and d indicate the reverse oxidation reactions. In the Li–S cells with LiFSI, the positively shifted peaks a and b and negatively shifted peaks c and d are observed, accompanied by an increase in peak currents. These findings suggest that LiFSI accelerates both the discharge and the charge kinetics of Li–S batteries and reduces the overpotential. Furthermore, Tafel slope analysis demonstrates the lowest Tafel slopes of the cells with LiFSI, measuring 37.5, 75.9, 42.5, and 96.0 mV dec^{-1} for the peaks a, b, c, and d respectively, supporting the enhanced cathode kinetics as well (Figure S14).

The Li–S battery performances are further measured with different Li salts. The Li–S cells with LiFSI exhibit superior rate performances with high specific capacities of 668 mAh g^{-1} at 3 C and 595 mAh g^{-1} at 4 C (1 C = 1672 mA g^{-1}), surpassing the cells with LiTFSI or LiBETI (Figure 6b and S15). More importantly, with the addition of LiFSI, Li–S batteries exhibit improved stability in long-term cycles. The Li–S cells with LiFSI deliver a long cycle lifespan of 1000 cycles at 2 C, while the cells with LiTFSI or LiBETI undergo rapid capacity decline and fail within only 150 or 250 cycles, respectively (Figure 6c and S16). The enhanced capacity retention of the Li–S cells with LiFSI is attributed to efficient utilization of the active energy materials enabled by the fast cathode kinetics.

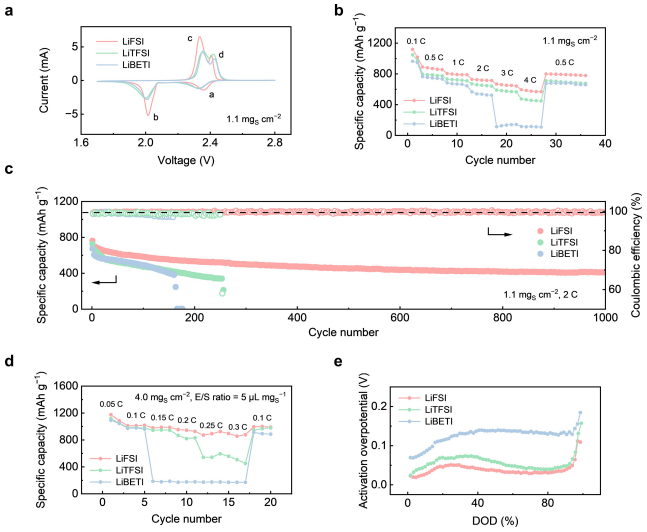

Figure 6. Performance evaluation of different Li salt anions on Li–S batteries. a) CV profiles of Li–S cells with 1.0 M LiFSI, LiTFSI or LiBETI. b) Rate performance and c) long-term cycle performance of Li–S cells with 1.0 M LiFSI, LiTFSI or LiBETI. d) Rate performance of Li–S cells with high areal sulfur loading cathodes and low E/S ratio and e) corresponding activation overpotential vs. depth of discharge (DOD) at 0.1 C discharge.

Furthermore, Li–S cells with high areal sulfur loading cathodes of 4.0 mg_S cm^{-2} and low electrolyte to sulfur (E/S) ratio of 5.0 μL mg_S^{-1} were assembled and tested under different rates to ascertain the capability of the anion regulation strategy under harsh working conditions. As shown in Figure 6d, the high-sulfur-loading Li–S cells with LiFSI demonstrate a specific capacity of 1176 mA g^{-1} at 0.05 C and maintain 896 mAh g^{-1} at a high discharge rate of 0.3 C. Conversely, the cells with LiTFSI or LiBETI exhibit sharply declined specific capacity at discharge rates of only 0.25 or 0.15 C. As revealed by the voltage–capacity curves, with the rise of the discharge rate, significantly increased polarization is observed in the cells with LiTFSI or LiBETI, and finally results in shortened discharge plateaus or premature discharge termination (Figure S17). In contrast, the cells with LiFSI demonstrate minimal polarization, delivering stable and prolonged discharge plateaus. The overpotential decoupling analysis further attributes the decreased polarization to the lowest activation overpotential of the cells with LiFSI (Figure 6e and S18), while the concentration overpotentials are similar for the different Li salts (Figure S19). This indicates that LiFSI accelerates the the intrinsic reaction kinetics of LiPSs by regulating the solvation structure of LiPSs and enables high-rate cycling with high areal sulfur loading cathodes and low electrolyte usage. A 3 Ah level Li–S pouch cell was further constructed to manifest the capability of LiFSI in practical use. The areal sulfur loading was 7.6 mg_S cm^{-2} for the pouch cell and an ultralow E/S ratio of 2.0 g g_S^{-1} was adopted. As shown in Figure S20, the Li–S pouch cell with LiFSI achieves a high energy density of 403 Wh kg^{-1} at 0.05 C with superior discharge capacity of 1195 mAh g^{-1}, demonstrating the effectiveness of regulating the anion structure to achieve high-energy-density Li–S batteries.

Conclusion

Li salt anions are found to be significantly involved in the solvation structure of LiPSs in Li–S batteries. Spectroscopy analysis identifies that Li salt anions participate prominently in the first solvation sheath of LiPSs. Further theoretical calculations and quantitative conductivity analysis demonstrate the strong tendency to form contact ion pairs between LiPS cations and Li salt anions in electrolyte. The anion solvation effect predominantly regulates the structure and formation energy of the solvated LiPS species and correspondingly the intrinsic kinetics of sulfur conversion reactions and the performances of Li–S batteries. Specifically, the addition of LiFSI to Li–S batteries reduces cell polarization, enhances rate performances, and achieves high-energy-density Li–S pouch cells. This work comprehensively

advances the understanding of the solvation chemistry in Li–S batteries, and highlights the promising potential of rational electrolyte designing for constructing high performance practical Li–S batteries.

Supporting Information

The authors have cited additional references within the Supporting Information.

Acknowledgements

This work was supported by National Key Research and Development Program (2021YFB2500300, 2021YFB2400300) and National Natural Science Foundation of China (22109007, 22109086, T2322015). The authors acknowledged the support from Tsinghua National Laboratory for Information Science and Technology for theoretical simulations. We thank Zheng Li, Xi-Yao Li, Chang-Xin Zhao, Chen-Xi Bi, and Zi-Xian Chen for the helpful discussion.

Conflict of Interest

The authors declare no conflict of interest.

Data Availability Statement

The data that support the findings of this study are available from the corresponding author upon reasonable request.

Keywords: Lithium–sulfur batteries · lithium polysulfides · solvation structure · electrolyte · lithium salt

[1] a) M. Zhao, B. Q. Li, X. Q. Zhang, J. Q. Huang, Q. Zhang, *ACS Cent. Sci.* **2020**, *6*, 1095; b) Z. X. Chen, M. Zhao, L. P. Hou, X. Q. Zhang, B. Q. Li, J. Q. Huang, *Adv. Mater.* **2022**, *34*, 2201555; c) Q. Cheng, Z.-X. Chen, X.-Y. Li, L.-P. Hou, C.-X. Bi, X.-Q. Zhang, J.-Q. Huang, B.-Q. Li, *J. Energy Chem.* **2023**, *76*, 181.

[2] a) C. Barchasz, F. Molton, C. Duboc, J. C. Lepretre, S. Patoux, F. Alloin, *Anal. Chem.* **2012**, *84*, 3973; b) M. Cuisinier, P.-E. Cabelguen, S. Evers, G. He, M. Kolbeck, A. Garsuch, T. Bolin, M. Balasubramanian, L. F. Nazar, *J. Phys. Chem. Lett.* **2013**, *4*, 3227; c) K. H. Wujcik, J. Velasco-Velez, C. H. Wu, T. Pascal, A. A. Teran, M. A. Marcus, J. Cabana, J. Guo, D. Prendergast, M. Salmeron, N. P. Balsara, *J. Electrochem. Soc.* **2014**, *161*, A1100.

[3] a) Y. Gorlin, A. Siebel, M. Piana, T. Huthwelker, H. Jha, G. Monsch, F. Kraus, H. A. Gasteiger, M. Tromp, *J. Electrochem. Soc.* **2015**, *162*, A1146; b) M. Li, J. Lu, J. Shi, S. B. Son, D. Luo, I. Bloom, Z. Chen, K. Amine, *J. Am. Chem. Soc.* **2021**, *143*, 2185.

[4] a) F. Y. Fan, Y.-M. Chiang, *J. Electrochem. Soc.* **2017**, *164*, A917; b) Z.-X. Chen, Q. Cheng, X.-Y. Li, Z. Li, Y.-W. Song, F. Sun, M. Zhao, X.-Q. Zhang, B.-Q. Li, J.-Q. Huang, *J. Am. Chem. Soc.* **2023**, *145*, 16449; c) C.-X. Bi, L.-P. Hou, Z. Li, M. Zhao, X.-Q. Zhang, B.-Q. Li, Q. Zhang, J.-Q. Huang, *Energy Mater. Adv.* **2023**, *4*, 0010.

[5] M. Zhao, B. Q. Li, H. J. Peng, H. Yuan, J. Y. Wei, J. Q. Huang, *Angew. Chem. Int. Ed.* **2020**, *59*, 12636; *Angew. Chem.* **2020**, *132*, 12736.

[6] a) Y. Liu, Y. Elias, J. Meng, D. Aurbach, R. Zou, D. Xia, Q. Pang, *Joule* **2021**, *5*, 2323; b) X. Chen, Q. Zhang, *Acc. Chem. Res.* **2020**, *53*, 1992.

[7] a) Z. Li, L. P. Hou, N. Yao, X. Y. Li, Z. X. Chen, X. Chen, X. Q. Zhang, B. Q. Li, Q. Zhang, *Angew. Chem. Int. Ed.* **2023**, *62*, 202309968; *Angew. Chem.* **2023**, *135*, 202309968; b) Q. Zou, Y. C. Lu, *EcoMat* **2021**, *3*, 12115; c) C. Yan, H.-R. Li, X. Chen, X.-Q. Zhang, X.-B. Cheng, R. Xu, J.-Q. Huang, Q. Zhang, *J. Am. Chem. Soc.* **2019**, *141*, 9422.

[8] a) A. Gupta, A. Bhargav, J.-P. Jones, R. V. Bugga, A. Manthiram, *Chem. Mater.* **2020**, *32*, 2070; b) A. Gupta, A. Bhargav, A. Manthiram, *Adv. Energy Mater.* **2019**, *9*, 1803096; c) X. Gao, Z. Yu, J. Wang, X. Zheng, Y. Ye, H. Gong, X. Xiao, Y. Yang, Y. Chen, S. E. Bone, L. C. Greenburg, P. Zhang, H. Su, J. Affeld, Z. Bao, Y. Cui, *Proc. Nat. Acad. Sci.* **2023**, *120*, 2301260120.

[9] a) Q. Pang, A. Shyamsunder, B. Narayanan, C. Y. Kwok, L. A. Curtiss, L. F. Nazar, *Nat. Energy* **2018**, *3*, 783; b) H. Ji, Z. Wang, Y. Sun, Y. Zhou, S. Li, J. Zhou, T. Qian, C. Yan, *Adv. Mater.* **2023**, *35*, 2208590.

[10] a) K. Nie, Q. Fu, R. Gao, K. Wang, H. Wang, C. Teng, X. Wang, J. Ren, R. Wang, *Energy Storage Mater.* **2023**, *63*, 103011; b) A. Gupta, A. Bhargav, A. Manthiram, *Chem. Mater.* **2021**, *33*, 3457.

[11] a) X. Zhu, T. Bian, X. Song, M. Zheng, Z. Shen, Z. Liu, Z. Guo, J. He, Z. Zeng, F. Bai, L. Wen, S. Zhang, J. Lu, Y. Zhao, *Angew. Chem. Int. Ed.* **2023**, *63*, 202315087; *Angew. Chem.* **2023**, *136*, 202315087; b) M. Zhao, B.-Q. Li, X. Chen, J. Xie, H. Yuan, J.-Q. Huang, *Chem* **2020**, *6*, 3297.

[12] a) J.-W. Park, K. Ueno, N. Tachikawa, K. Dokko, M. Watanabe, *J. Phys. Chem. C* **2013**, *117*, 20531; b) J.-W. Park, K. Yamauchi, E. Takashima, N. Tachikawa, K. Ueno, K. Dokko, M. Watanabe, *J. Phys. Chem. C* **2013**, *117*, 4431.

[13] a) M. Cuisinier, P. E. Cabelguen, B. D. Adams, A. Garsuch, M. Balasubramanian, L. F. Nazar, *Energy Environ. Sci.* **2014**, *7*, 2697; b) C.-W. Lee, Q. Pang, S. Ha, L. Cheng, S.-D. Han, K. R. Zavadil, K. G. Gallagher, L. F. Nazar, M. Balasubramanian, *ACS Cent. Sci.* **2017**, *3*, 605.

[14] L.-P. Hou, X.-Q. Zhang, N. Yao, X. Chen, B.-Q. Li, P. Shi, C.-B. Jin, J.-Q. Huang, Q. Zhang, *Chem* **2022**, *8*, 1083.

[15] a) K. Dokko, N. Tachikawa, K. Yamauchi, M. Tsuchiya, A. Yamazaki, E. Takashima, J.-W. Park, K. Ueno, S. Seki, N. Serizawa, M. Watanabe, *J. Electrochem. Soc.* **2013**, *160*, A1304; b) L. Wang, Y. Xie, X. Qi, R. Jiang, K. Huang, L. Qie, S. Li, *ACS Appl. Mater. Interfaces* **2022**, *14*, 46457.

[16] a) Q. Zou, Y. C. Lu, *J. Phys. Chem. Lett.* **2016**, *7*, 1518; b) M. Cuisinier, C. Hart, M. Balasubramanian, A. Garsuch, L. F. Nazar, *Adv. Energy Mater.* **2015**, *5*, 1401801; c) E. P. Kamphaus, P. B. Balbuena, *J. Phys. Chem. C* **2021**, *125*, 20157.

[17] a) N. N. Rajput, V. Murugesan, Y. Shin, K. S. Han, K. C. Lau, J. Z. Chen, J. Liu, L. A. Curtiss, K. T. Mueller, K. A. Persson, *Chem. Mater.* **2017**, *29*, 3375; b) C. Park, A. Ronneburg, S. Risse, M. Ballauff, M. Kanduc, J. Dzubiella, *J. Phys. Chem. C* **2019**, *123*, 10167; c) N. Yao, X. Chen, X. Shen, R. Zhang, Z. H. Fu, X. X. Ma, X. Q. Zhang, B. Q. Li, Q. Zhang, *Angew. Chem. Int. Ed.* **2021**, *60*, 21473; *Angew. Chem.* **2021**, *133*, 21643.

[18] a) F. Y. Fan, M. S. Pan, K. C. Lau, R. S. Assary, W. H. Woodford, L. A. Curtiss, W. C. Carter, Y.-M. Chiang, *J. Electrochem. Soc.* **2016**, *163*, A3111; b) B. Yang, H. Jiang, Y. Zhou, Z. Liang, T. Zhao, Y.-C. Lu, *ACS Appl. Mater. Interfaces* **2019**, *11*, 25940; c) H. Moon, T. Mandai, R. Tatara, K. Ueno, A.

Yamazaki, K. Yoshida, S. Seki, K. Dokko, M. Watanabe, *J. Phys. Chem. C* **2015**, *119*, 3957; d) Q. He, Y. Gorlin, M. U. M. Patel, H. A. Gasteiger, Y. C. Lu, *J. Electrochem. Soc.* **2018**, *165*, A4027.
[19] Y.-W. Song, L. Shen, N. Yao, X.-Y. Li, C.-X. Bi, Z. Li, M.-Y. Zhou, X.-Q. Zhang, X. Chen, B.-Q. Li, J.-Q. Huang, Q. Zhang, *Chem* **2022**, *8*, 3031.
[20] M. Shin, H.-L. Wu, B. Narayanan, K. A. See, R. S. Assary, L. Zhu, R. T. Haasch, S. Zhang, Z. Zhang, L. A. Curtiss, A. A. Gewirth, *ACS Appl. Mater. Interfaces* **2017**, *9*, 39357.
[21] K. A. See, H.-L. Wu, K. C. Lau, M. Shin, L. Cheng, M. Balasubramanian, K. G. Gallagher, L. A. Curtiss, A. A. Gewirth, *ACS Appl. Mater. Interfaces* **2016**, *8*, 34360.
[22] D. M. Seo, P. D. Boyle, R. D. Sommer, J. S. Daubert, O. Borodin, W. A. Henderson, *J. Phys. Chem. B* **2014**, *118*, 13601.
[23] a) C. Capiglia, N. Imanishi, Y. Takeda, W. A. Henderson, S. Passerini, *J. Electrochem. Soc.* **2003**, *150*, A525; b) S.-D. Han, R. D. Sommer, P. D. Boyle, Z.-B. Zhou, V. G. Young, O. Borodin, W. A. Henderson, *J. Electrochem. Soc.* **2022**, *169*, 110544.
[24] X. Chen, X. Q. Zhang, H. R. Li, Q. Zhang, *Batteries & Supercaps* **2019**, *2*, 128.
[25] R. Raccichini, J. W. Dibden, A. Brew, J. R. Owen, N. Garcia-Araez, *J. Phys. Chem. B* **2018**, *122*, 267.
[26] S. Feng, Z. H. Fu, X. Chen, B. Q. Li, H. J. Peng, N. Yao, X. Shen, L. Yu, Y. C. Gao, R. Zhang, Q. Zhang, *Angew. Chem. Int. Ed.* **2022**, *61*, 202211448; *Angew. Chem.* **2022**, *134*, 202211448.

Manuscript received: January 5, 2024
Accepted manuscript online: February 7, 2024
Version of record online: February 28, 2024